Available online at www.sciencedirect.com

jmr&t
Journal of Materials Research and Technology

journal homepage: www.elsevier.com/locate/jmrt

Original Article

Evaluation of flexural properties and characterisation of 10-mm thin geopolymer based on fly ash and ladle furnace slag

Ng Yong-Sing [a,b], Liew Yun-Ming [a,b,*], Heah Cheng-Yong [a,c], Mohd Mustafa Al Bakri Abdullah [a,b], Lynette Wei Ling Chan [d], Ng Hui-Teng [a,b], Ong Shee-Ween [a,b], Ooi Wan-En [a,b], Hang Yong-Jie [a,b]

[a] Centre of Excellence Geopolymer and Green Technology (CeGeoGTech), Universiti Malaysia Perlis (UniMAP), Kangar, 01000, Perlis, Malaysia
[b] Faculty of Chemical Engineering Technology, Universiti Malaysia Perlis (UniMAP), Kangar, 01000, Perlis, Malaysia
[c] Faculty of Mechanical Engineering Technology, Universiti Malaysia Perlis (UniMAP), Kangar, 01000 Perlis, Malaysia
[d] Ceramic Research Company Sdn Bhd (Guocera-Hong Leong Group), Lot 7110, 5 ½ Miles, Jalan Kapar, 42100, Klang, Selangor, Malaysia

ARTICLE INFO

Article history:
Received 11 May 2021
Accepted 6 August 2021
Available online 12 August 2021

Keywords:
Thin
Geopolymer
Flexural properties
Formulation
Ladle furnace slag

ABSTRACT

The formulation and flexural properties of thin fly ash geopolymers with thickness of merely 10 mm and replacement of ladle furnace slag to fly ash in thin geopolymer were presented. The formulation was discussed in terms of NaOH molarity, solid aluminosilicates-to-liquid alkali activator (S/L) mass ratio, and alkali activator (Na_2SiO_3/NaOH) mass ratio. Thin fly ash geopolymers with flexural strength and Young's modulus of 6.2 MPa and 0.14 GPa, respectively, were obtained by using 12 M NaOH, S/L ratio of 2.5 and Na_2SiO_3/NaOH ratio of 4.0. A high Na_2SiO_3/NaOH ratio was implemented for thin geopolymer synthesis to produce a more viscous slurry which helped to retain the shape of a thin geopolymer. The incorporation of ladle furnace slag up to 40 wt.% reported an increment of 26% in flexural strength up to 7.8 MPa as compared to pure fly ash geopolymers and the stiffness was increased to 0.19 GPa. Denser microstructure with improved compactness was observed as the ladle furnace slag acted as the filler. New crystalline phases of calcium silicate hydrate (C–S–H) were formed and coexisted with the geopolymer matrix, which consequently enhanced the flexural strength of thin fly ash geopolymer. This proved that the ladle furnace slag has the potential to be utilised in geopolymer synthesis and will enhance the flexural properties of thin geopolymers. The flexural performance of thin geopolymers in this study was considerably good as the thin geopolymers exhibited comparatively similar flexural strengths, but a higher strength/thickness ratio as compared to geopolymers with thickness greater than 40 mm.

* Corresponding author.
E-mail address: yun86_liew@yahoo.com (L. Yun-Ming).

https://doi.org/10.1016/j.jmrt.2021.08.016

1. Introduction

Geopolymers are inorganic polymers formed by the polycondensation of solid aluminosilicate in a highly alkaline medium through geopolymerisation process [1]. The types of solid aluminosilicate-based materials could be divided into natural materials, such as kaolin [2] and metakaolin [3] or industrial by-products, such as fly ash [4] and slag [5]. The geopolymerisation reaction process involves multi-steps that occur simultaneously, which include the dissolution of Si and Al species from aluminosilicate precursors, followed by polycondensation of soluble species to form aluminosilicate gel phases and eventually gel hardening to form a rigid solid [6]. Geopolymers have a three-dimensional structure of the Si–O–Al polymeric network, whereby the Al is in four-fold coordination [7]. This three-dimensional framework of SiO_4 and AlO_4 gives geopolymer the ceramic-like characteristics and exhibits excellent physical and mechanical properties [8].

The incorporation of two or more precursor aluminosilicates could produce geopolymers with better properties than precursors that are activated alone [9]. The mechanical strength of fly ash geopolymers could be improved by incorporating slag as the aluminosilicate source during the mixing process. Ladle furnace slag (LFS) possesses similar chemical composition (high calcium content) to ground granulated blast furnace slag (GGBFS), which is commonly used in geopolymer research. However, the incorporation of ladle furnace slag in geopolymer synthesis is still very limited as compared to ground granulated blast furnace slag. The current application of ladle furnace slag included water depuration, soil stabilisation, masonry mortars, road construction and bituminous mixes [10]. Nevertheless, Wang et al. [11] studied the engineering properties of ladle furnace slag and obtained a compressive strength of 15 MPa in the geopolymer produced. Murri et al. [12] compared the strength performances of metakaolin/LFS geopolymer with fly ash/LFS geopolymer and observed that the metakaolin/LFS geopolymer exhibited a higher compressive strength of 44 MPa than fly ash/LFS geopolymer (11 MPa). These studies showed that ladle furnace slag had cementitious properties and has the potential in enhancing the strength properties of geopolymers.

Thus far, research studies regarding the flexural properties of geopolymers were mainly focused on precast concrete elements such as beams and columns, which were thicker. Most research studies regarding geopolymer concrete have thickness of ~70 mm–100 mm with the addition of aggregates and fibers [13–15]. Besides, geopolymers which were utilised in coating fields were mainly focused on adhesive strength [16], while studies regarding geopolymer membrane (5 mm–20 mm) were less focused on the mechanical properties or were only taking measurement in compressive strength [17,18]. For instance, thin geopolymer has also been investigated by several researchers [19,20]. Based on Kumar et al. [19], thin fly ash/slag geopolymers with thickness of 25 mm were cured at room temperature for 24 h and followed by heat treatment at 150 °C–300 °C. The compressive strength of 20–50 MPa was reported. On the other hand, Suzuk et al. [20] prepared thin metakaolin geopolymer with 10-mm thickness using pressing and extrusion method. The samples were cured at 60 °C for 2 h followed by 20 °C for 24 h and rupture strength of 11–14.4 MPa was reported.

In order to produce thin geopolymer, the mixing parameters are one of the key factors. Generally, the alkali solution molarity and mixing ratio in terms of solid-to-liquid and alkali silicate-to-alkali solution are common parameters to determine the formulation of geopolymers with cuboid and cube-shaped and their influences were well-reported [21–23]. Even so, these parameters are crucial for the formation of thin geopolymers as the workability, setting and shaping [22,24] of geopolymers are significantly dependent on these mixing parameters. Thin geopolymers could not harden or experience bending if these parameters are not optimised. Besides, the flexural properties of geopolymer are related to these mixing parameters as they influence the dissolution and polycondensation extent of geopolymers [6]. Since the study with regard to properties of thin neat geopolymers is still very limited, there is an urge to study the relationship between formulations with flexural properties of thin geopolymers. Flexural properties of thin geopolymers is significant as it could determine the functionality of thin geopolymers to be utilised in various application such as floor imprint, roof tiles, thin wall panels, geopolymer composite membranes and especially tiles manufacturing for flooring and wall. As geopolymer is brittle in nature, flexural strength is more representative in identifying the capacity of deformation resistance and strength retention especially to thin geopolymer with only 10 mm thickness.

To recap, the research regarding the thin neat geopolymer with 10-mm thickness is less reported. The flexural strength properties of geopolymer is less focused in most research compared to compressive strength properties. Moreover, the inclusion of ladle furnace slag in geopolymer synthesis is very little. Thus, the investigation and formulation of the thin geopolymers are essential to addressing the warping and hardening problems, as aforementioned, and to explore the usefulness for application. Therefore, this paper investigated the formulation of thin fly ash geopolymers in terms of NaOH molarity, solid aluminosilicates-to-liquid alkali activator (S/L) mass ratio and Na_2SiO_3/NaOH mass ratio. The effect of ladle furnace slag as partial replacement in the thin geopolymer was also evaluated. The flexural properties of thin fly ash geopolymers with incorporation of ladle furnace slag was comprehensively studied to access the feasibility of thin geopolymers. The effect of varying mixing parameters and partial replacement by ladle furnace slag on the fly ash geopolymers has been reported in our previous paper [25]. The outcome of the paper is vital as it would expand the utilisation of thin geopolymers in terms of flexural properties and increase the application of ladle furnace slag in geopolymer synthesis.

Table 1 – Chemical composition of fly ash and ladle furnace slag.

Compound	SiO_2	Al_2O_3	CaO	Fe_2O_3	MgO	TiO_2	K_2O	Others
FA (wt.%)	56.30	28.00	3.89	6.86	–	2.17	1.49	1.29
LFS (wt.%)	21.30	2.30	63.59	8.08	2.60	0.50	–	1.63

2. Methodology

2.1. Materials

Fly ash (FA) collected from Sultan Azlan Shah Power Station, TNB Janamanjung Sdn. Bhd., Seri Manjung, Perak, Malaysia, and ladle furnace slag (LFS) collected from Southern Steel Berhad Penang, Malaysia, were used as the aluminosilicate sources in this study. The chemical composition of FA and LFS obtained through X-Ray Fluorescence (XRF) analysis is tabulated in Table 1. The fly ash was made up mainly of SiO_2 (56.30 wt.%) and Al_2O_3 (28.00 wt.%) while the ladle furnace slag consisted of a high amount of CaO (63.59 wt.%) with 21.30 wt.% of SiO_2 and 2.30 wt.% of Al_2O_3. The fly ash used was classified as Class F fly ash in accordance with ASTM C618 as the CaO content was less than 18 wt.% (3.89 wt.%). Fig. 1 depicts the microstructure of FA and LFS particles. The FA particles are spherical with smooth surfaces while LFS has irregular and angular shape with sharp-edged and partly dense grains.

Both liquid sodium silicate (Na_2SiO_3) and sodium hydroxide (NaOH) solution were mixed to prepare the alkali activator. The liquid sodium silicate (Na_2SiO_3) (South Pacific Chemicals Industries Sdn. Bhd., Malaysia) is made up mainly of 30.1 wt.% of SiO_2, 9.4 wt.% of Na_2O and 60.5 wt.% of H_2O, with modulus $SiO_2/Na_2O = 3.2$, specific gravity and viscosity of 1.4 g/cm^3 and 0.4 Pa s respectively at 20 °C. Caustic soda pellets (HmbG® Chemicals, Sigma-Alrich Germany) with the assay of 97% were mixed with distilled water to prepare NaOH solution.

2.2. Formation of thin geopolymers

In this study, the formulation of thin geopolymers was investigated in terms of NaOH molarity, S/L mass ratio and sodium silicate-to-sodium hydroxide (Na_2SiO_3/NaOH) mass ratio. Table 2 summarises the mixing parameters for the formulation of thin fly ash geopolymers. The S/L ratio and Na_2SiO_3/NaOH ratio of 2.5 were fixed at the initial experiment as the ratios were pre-determined from the trial and error experimental works as the thin geopolymers produced using these ratios could harden and did not experience excessive bending after the curing process. For the investigation on the effect of S/L ratio, S/L ratio of 3.2 was set as the upper boundary of this experimental work as the mixing process beyond that was undesirable due to low workability where slurry form of mixture cannot be achieved. The optimum value for each parameter was carried forward to the next experimental work.

Thin fly ash/slag geopolymers was prepared by using fly ash and ladle furnace slag as the aluminosilicate sources. Portion of fly ash was replaced with ladle furnace slag. The weight percentage of ladle furnace slag replacement was set as shown in Table 2. Fly ash and ladle furnace slag were dry mixed and then mixed with the liquid alkali activator until homogenous slurry was achieved. The fresh slurry was then rapidly moulded and compacted into 160 × 40 × 10 mm moulds according to ASTM C109. The thin geopolymer samples were cured at 60 °C in the oven for 6 h. The samples were further cured for another 24 h at room temperature. The cured samples (Fig. 2) were kept at room temperature for 28 days.

2.3. Testing and analysis

The bulk density measurement was evaluated using the mass and dimension of the samples based on BS EN 12390-7. The water absorption and apparent porosity were determined using wet mass (M_w), dry mass (M_d) and suspended mass (M_s) according to ASTM C642 as shown in Eqs. (1) and (2).

$$\text{Water Absorption} = \frac{Mw - Md}{Md} \quad (1)$$

$$\text{Apparent Porosity} = \frac{Mw - Md}{Mw - Ms} \quad (2)$$

The flexural test was assessed using Instron Machine Series 5569 Mechanical Tester in accordance with ASTM C348.

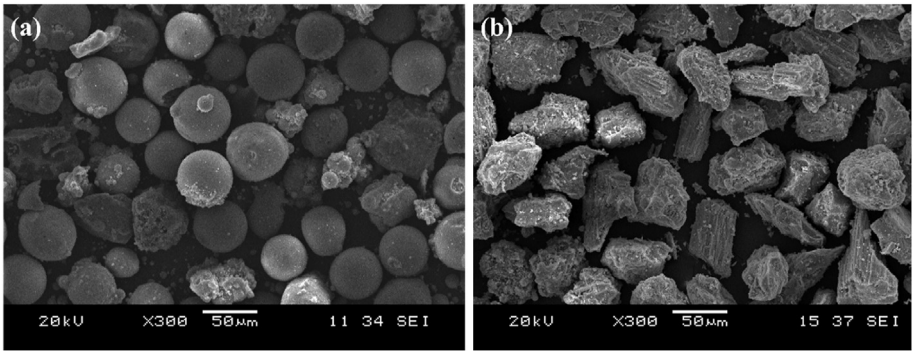

Fig. 1 – SEM micrographs of (a) FA and (b) LFS.

Table 2 – Details of mixture proportions.

Type of Geopolymers	NaOH Molarity	S/L Ratio	Na_2SiO_3/NaOH Ratio	LFS Replacement (wt.%)
Thin Fly Ash Geopolymer	6 M, 8 M, 10 M, 12 M, 14 M	2.5	2.5	–
	12M	1.5, 2.0, 2.5, 3.0, 3.2	2.5	–
	12 M	2.5	2.0, 2.5, 3.0, 3.5, 4.0, 4.5	–
Thin Fly Ash/Slag Geopolymer	12 M	2.5	4.0	10, 20, 30, 40

Value in grey boxes indicates the optimum value carried forward from the previous experimental works.

The span length was fixed at 110 mm with 1 mm/min of crosshead speed. The flexural strength and Young's modulus were calculated using Eqs. (3) and (4), respectively. 5 samples were tested for each parameter and the average value of flexural strength and Young's modulus was obtained to minimize the random error.

$$\text{Flexural Strength} = \frac{3FL}{2bd^2} \quad (3)$$

$$\text{Young's Modulus} = \frac{L^3m}{4bd^3} \quad (4)$$

where F = load at a given point on the load deflection curve, (kg/m^2), L = support span length (mm), b = width of specimens (mm), d = thickness of specimens (mm), and m = gradient of the initial straight-line portion in load deflection curve (N/mm).

JSM-6460LA model Scanning Electron Microscope (JEOL) was performed to reveal the microstructure of the thin geopolymer. The fracture surface was cut into small pieces and coated with a thin layer of platinum using JEOL JFC 1600 Auto Fine Coater to prevent electrostatic charge during imaging.

The phase analysis of fly ash, ladle furnace slag and thin geopolymers was identified using D2 Phaser, Bruker X-Ray Diffractometer with Cu-Kα radiation operated at 40 kV and 35 mA. The scan range and scan rate were fixed at 10–80°2θ and 2°2θ per minute, respectively. X'pert High Score Plus software equipped with ICDD PDF-2 database was used to analyze the XRD patterns.

Perkin Elmer Fourier Transform Infrared Spectroscopy (FTIR) RXI spectrometer was used to determine the functional group of geopolymers. The samples were scanned from 650 cm^{-1} to 4000 cm^{-1} with a resolution of 4 cm^{-1}.

3. Results and discussion

3.1. *Bulk density, apparent porosity and water absorption*

Fig. 3 displays the bulk density, apparent porosity, and water absorption of thin fly ash geopolymers with various parameters. The bulk densities of thin geopolymers increased to an optimal and then reduced. The change in density, porosity and water absorption was not significant. The mixture is sticky in order to avoid excessive warping and bending of geopolymer specimen, which finally causes small changes in the bulk density, porosity and water absorption [22]. In general, the values of bulk density, apparent porosity, and water absorption complied with each other, as denser geopolymers produced geopolymer structures with lesser pore structure and reduced the apparent porosity and water absorption.

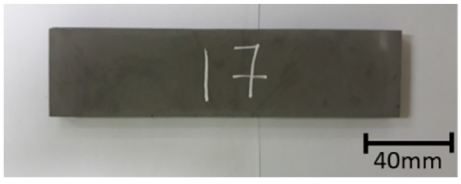

Fig. 2 – Thin fly ash geopolymers after 28 days.

The range of bulk density of thin fly ash geopolymers (Fig. 3a–c) fell between 1702 and 2061 kg/m^3. The bulk density range was commonly reported for fly ash geopolymers [26]. The apparent porosity and water absorption of thin fly ash geopolymers ranged from 19.3 to 23.1% and 9.9–12.4%, respectively, were lower as compared to fly ash geopolymers [27]. This was associated with the shape and thickness of geopolymers and the higher Na_2SiO_3/NaOH used in this study because the silicates increased the mixture flow and occupied the voids present between the fly ash particles [28].

The changes of bulk density, apparent porosity, and water absorption of fly ash geopolymers were relatively more significant with differing S/L and Na_2SiO_3/NaOH ratios. Both ratios markedly affected the fluidity and workability of geopolymer slurry, whereby high workable slurry was achieved with lower S/L and Na_2SiO_3/NaOH ratios. However, when the liquid content was too high, the intermolecular contact between aluminosilicates and alkali activator could be potentially hindered. The polycondensation reaction consequently became less efficient and more pores were produced in the geopolymer matrix due to the evaporation of moisture [29]. In contrast, as both S/L and Na_2SiO_3/NaOH ratios exceeded the optimal values, the liquid content became too low and caused higher porosity due to the low workable slurry, which prohibited proper paste consolidation and promoted pore formation [22]. On the other hand, increasing NaOH molarity produced denser geopolymer with lower porosity and water absorption (Fig. 3a). This was associated with the rise in the degree of dissolution of the active species from precursors in high NaOH concentration which facilitated the formation of geopolymer network [21]. Nevertheless, the bulk density decreased slightly at 14 M NaOH as the occurrence of disruption of ion mobility and ion species stability [30].

Based on Fig. 3d, the bulk density of thin fly ash/slag geopolymers (2097–2273 kg/m^3) was slightly higher than the optimised fly ash geopolymer (2061 kg/m^3). This was associated with the comparatively higher density of ladle furnace slag precursors (1238 kg/m^3) than fly ash (1168 kg/m^3). Nevertheless, the changes in bulk density was considerably little (1.8–10.3%) as the ladle furnace slag was added as partial replacement [31]. Furthermore, both the apparent porosity (16.1%–18.4%) and water absorption (8.2%–9.7%) of thin fly

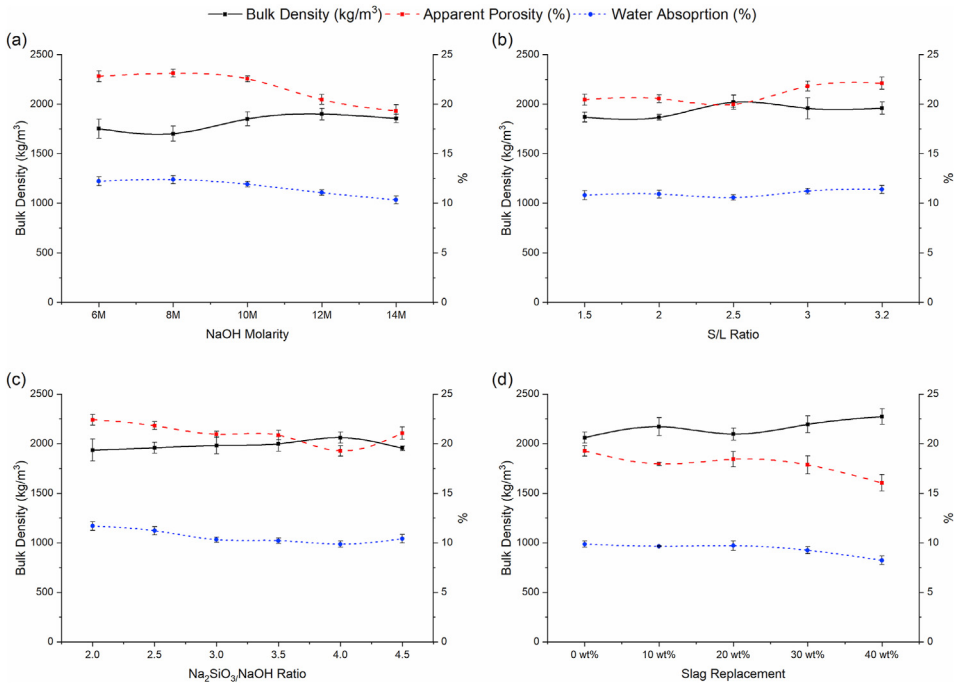

Fig. 3 – Bulk density, apparent porosity and water absorption of thin fly ash geopolymer with varying (a) NaOH molarity, (b) S/L ratio, (c) Na_2SiO_3/NaOH ratio and (d) slag replacement.

ash/slag geopolymers were lower than the fly ash geopolymers. In comparison, the thin fly ash/slag geopolymer in this study had higher bulk density and lower porosity relative to other research studies. For instance, Ababneh et al. [32] reported a density of 1980 kg/m^3–2030 kg/m^3 and porosity of 27%–34% for FA/GGBFS-based geopolymers with 15 wt.% GGBFS addition. Besides, according to Song et al. [33], fly ash/electric furnace steel slag geopolymers with slag content of 10 wt.%–50 wt.% had density ranged from 1691 kg/m^3–1859 kg/m^3 and porosity of 33.8%–35.8%. A lower density of 1280–1700 kg/m^3 with higher porosity of 23.6%–38.6% was reported by Bignozzi et al. [34] in metakaolin/ladle furnace

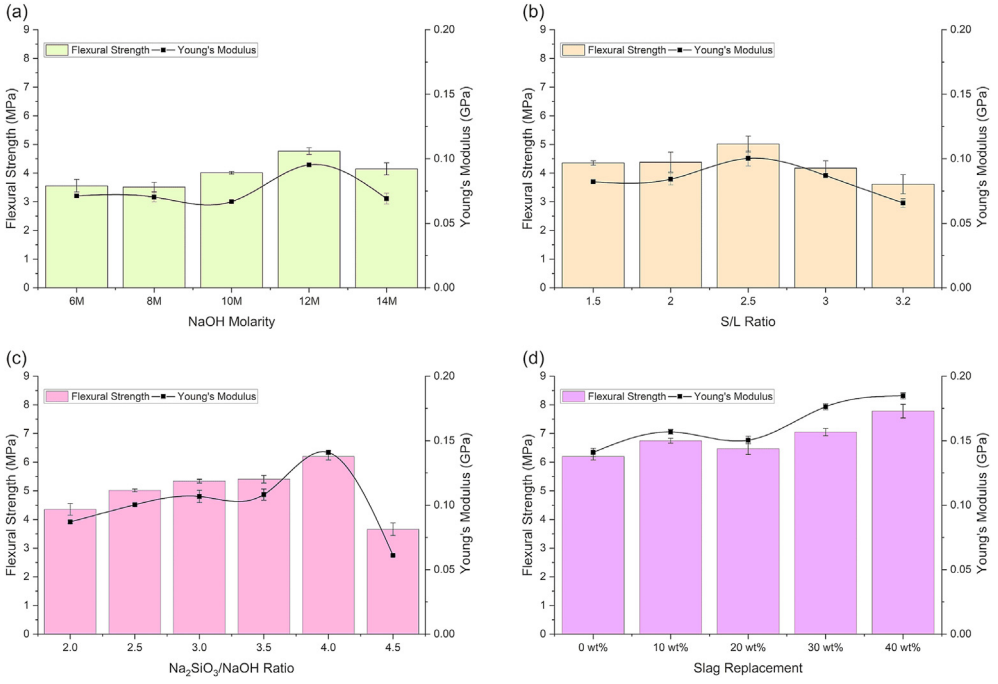

Fig. 4 – Flexural strength and Young's modulus after 28 days of thin fly ash geopolymer with varying (a) NaOH molarity, (b) S/L ratio, (c) Na_2SiO_3/NaOH ratio and (d) slag replacement.

slag geopolymers with incorporation of 25 wt.% –50 wt.% of slag. These studies also showed small changes in bulk density (1.7%–15.9%) due to addition of slag as partial replacement, as aforementioned.

3.2. *Flexural strength and Young's modulus*

3.2.1. *Thin fly ash geopolymers*

Mixing parameters are significant in determining the mechanical properties of thin fly ash geopolymers as they influence the geopolymerisation extent and geopolymer matrix formation. Based on Fig. 4a–c, the thin fly ash geopolymers synthesised by using 12 M NaOH molarity, S/L ratio of 2.5 and Na_2SiO_3/NaOH ratio of 4.0 had the optimum flexural strength of 6.2 MPa and Young's Modulus of 0.13 GPa. In general, the increase in mixing parameters led to the rise in flexural strength up to an optimal but then reduced beyond the optimal ratio. The flexural strength differed by 41.0%, 28.0% and 26.2% with changes of Na_2SiO_3/NaOH ratio, S/L ratio and NaOH molarity, respectively, demonstrating that the strength determining factor was Na_2SiO_3/NaOH ratio > S/L ratio > NaOH molarity. Young's modulus increased with increasing flexural strength.

The Na_2SiO_3/NaOH ratio (Fig. 4c) was the key parameter in thin geopolymer formation followed by S/L ratio (Fig. 4b) and NaOH molarity (Fig. 4a) due to the higher variability in the flexural strength. The optimum Na_2SiO_3/NaOH ratio of 4.0 for thin geopolymer obtained in this study was comparatively higher than cubic geopolymer [35,36], which usually ranged from 0.05 to 3.00. Increasing Na_2SiO_3/NaOH ratio induced more soluble Si species while decreasing Na_2SiO_3/NaOH ratio had more OH^- species for dissolution [37]. The high Na_2SiO_3/NaOH ratio promoted the formation of mobile precursors, which improved the reaction kinetics by increasing the geopolymerisation extent [23], and thus enhanced the flexural strength and stiffness of thin geopolymers. Most importantly, the high Na_2SiO_3/NaOH ratio produced a more viscous slurry which could help to retain the shape of thin geopolymers and avoid bending in the sample. However, when exceed the optimal Na_2SiO_3/NaOH ratio, precipitation of Al–Si phase occurred with excess sodium silicate content, which prohibited the contact between the precursor material and alkaline activator, and hindered the structure formation during the polycondensation process.

Based on Fig. 4b, the ideal S/L ratio reported in this study was 2.5, which indicated the occurrence of proper dissolution of fly ash particles, and the optimal frequency of contact between alkaline activator and fly ash. A higher liquid content (low S/L ratio) caused the formation of less viscous slurry [22], which created a tension force on the sample surface and caused the curvature in the sample, as shown in Fig. 5, hence, it resulted in a lower flexural strength. In contrast, high solid content (high S/L ratio) caused undesirable mixing and was difficult in thin mould compaction. The low fluidity retarded the proper consolidation of paste and lowered the flexural performance of thin geopolymer [38].

Besides, the results showed that a higher NaOH molarity of 12 M (Fig. 4a) was required for higher flexural strength and stiffness development in thin geopolymer. More reactive bonds for monomers were formed which enhanced the intermolecular bonding strength of geopolymers [21]. However, premature precipitation of the geopolymer matrix occurred beyond its optimal NaOH molarity [30], as the result of faster condensation and led to lower strength and stiffness. In contrast, a lower NaOH molarity had lower Na^+ and OH^- ions for the dissolution of fly ash particles [27].

3.2.2. *Thin fly ash/slag geopolymers*

Referring to Fig. 4d, the flexural strength and Young's modulus showed an increasing trend with an increasing amount of ladle furnace slag replacement. The highest flexural strength of 7.8 MPa with enhancement by 26% as compared to pure fly ash geopolymers and highest stiffness of 0.19 GPa were achieved with the proportion of fly ash to slag of 60:40. The substitution of ladle furnace slag into fly ash geopolymers accelerated the reaction rate and promoted strength development [39]. Besides, the CaO content from ladle furnace slag induced Ca^{2+} ions into geopolymer system, and promoted the formation of C–S–H gel (Calcium Silicate Hydrate) alongside N–A–S–H (Sodium Aluminosilicate Hydrate) gel [40]. Nevertheless, a slight drop in the flexural strength and stiffness was observed in the fly ash/slag geopolymer with the mixing proportion of 80:20, which may be resulted by the decreased bulk density and increased pores as shown in Fig. 3d.

The flexural strength of thin fly ash/slag geopolymers performed slightly better than the fly ash/slag geopolymers synthesised by other researchers. For instance, Nath and Sarker [13] and Fang et al. [41] produced fly ash/GGBFS geopolymers with flexural strength of 4.5 MPa–6.1 MPa and 1.4 MPa–3.6 MPa, respectively. Besides, flexural strength of 4.6 MPa–5.8 MPa was reported by Gülşan et al. [42] for fly ash/GGBFS geopolymer reinforced with steel. Song et al. [33] reported flexural strength of 2.61 MPa and 3.95 MPa for fly ash/steel slag geopolymers cured at 7 days and 28 days, respectively. However, based on Cifrian et al. [43], the fly ash/clay geopolymer added with electric arc furnace dust cured at 75 °C reported a flexural strength of 16.4 MPa. This might be associated with the high curing temperature and high Fe_2O_3 content (33.36 wt.%) of the electric arc furnace dust. Nevertheless, the enhancement of flexural behaviour by incorporating ladle furnace slag into geopolymer synthesis was possible based on the flexural results obtained.

3.3. *Effect of thickness on flexural strength*

Table 3 compares the flexural strength and Young's modulus of thin geopolymers obtained in this study with those reported by other researchers. The thickness of the specimen would affect the flexural strength of the final product. In general, increasing thickness of specimen will lead to a higher

Fig. 5 – Curved thin fly ash geopolymer synthesised with S/L ratio of 1.5.

Table 3 – Comparison of thin geopolymers in terms of flexural strength, Young's modulus, thickness, and strength/thickness ratio with other researchers.

Reference	Precursors	Aggregates	Fillers/Additives	Flexural Strength (MPa)	Young's Modulus (GPa)	Thickness (mm)	Strength/Thickness Ratio
This study	FA	–	–	*6.2	0.13	10	0.62
This study	FA, LFS	–	–	*7.8	0.19	10	0.78
Song et al. [33]	FA, electric furnace steel slag	–	–	*1.6–4.0	3.5–4.4	40	0.04–0.1
Elyamany et al. [47]	FA, GGBFS	–	Silica fume	*3.0–7.4	–	40	0.075–0.185
Nazari et al. [48]	FA, anhydrous borax	–	Steel fiber	*5.0–9.5	–	40	0.125–0.238
Al-Qutaifi et al. [49]	FA	Sand	Steel fiber, polypropylene fiber	*2.8–6.2	–	40	0.07–0.155
Mucsi et al. [50]	FA	–	Waste tire fiber, steel fiber	*1.1–2.7	–	40	0.028–0.068
Saafi et al. [51]	FA	–	Graphene	*3.1–7.8	0.5–2.5	50	0.062–0.156
Adak et al. [52]	FA	Sand	Nano-silica	*3.2–7.3	–	50	0.064–0.146
Tanyildizi & Yonar [14]	FA	River sand	Polyvinyl alcohol fiber	*3.9–7.8	–	75	0.052–0.104
Nath & Sarker [13]	FA, GGBFS	Fine, coarse aggregates	–	*4.5–6.1	17.4–23.2	100	0.045–0.061
Raut et al. [15]	FA, GGBFS	Fine, coarse aggregates	Basalt fiber	*2.4–5.1	21.1–26.9	100	0.024–0.051
Fang et al. [41]	FA, GGBFS	Sand, granite	–	*1.4–3.6	19–29.4	100	0.014–0.036
Mohseni [23]	Metakaolin	Fine, coarse aggregates	Polypropylene fiber	*7.0–9.8	–	100	0.07–0.098
Bhutta et al. [53]	FA	Fine aggregates	Steel fiber, polypropylene fiber	*1.4–2.9	–	100	0.014–0.029
Luhar et al. [54]	FA	Fine, coarse aggregates	Rubber fiber	*6.5–9.9	20.1–31.5	100	0.065–0.099
Gülşan et al. [42]	FA, GGBFS, nano-silica	Fine, coarse aggregates	Steel reinforcement	*4.6–5.8	–	150	0.031–0.039

The flexural strength value with * indicates geopolymer specimen without any additives/fillers (controlled specimen).

flexural strength [44]. With the thickness as thin as 10 mm, the range of flexural strength obtained in this study (6.2 MPa and 7.8 MPa for fly ash geopolymers and fly ash/slag geopolymer, respectively) was comparatively similar to those reported by other research works (1.4 MPa–9.9 MPa) with thickness greater than 40 mm. For comparison, the strength/thickness ratio was calculated as shown in Table 3. The fly ash geopolymer and fly ash/slag geopolymer investigated in this study showed a higher strength/thickness ratio of 0.62 and 0.78, respectively. This indicated that the flexural performance of thin geopolymer in this study was considerably good as the thin geopolymer could retain a similar load that was applied to thicker geopolymer.

Besides, the thin neat geopolymers (without the addition of fillers and aggregates) in this study exhibited higher flexural strength as compared to other researchers' geopolymer specimens without additives or fillers (the flexural value was denoted with * in Table 3). Yet, this again was related to the higher Na_2SiO_3/NaOH ratio used in this study as aforementioned and proved that the thin geopolymers in this study have the potential to be explored in various applications such as tile industry (floor tiles, wall tiles), floor imprint, roof tiles, thin wall panels and geopolymer composite membranes. However, further work should be carried out to increase the flexural strength of thin geopolymers to enhance the versatility of thin geopolymers.

On the other hand, Young's modulus results showed an increasing trend with increasing thickness based on Table 3. Stiffness of 0.13 GPa and 0.19 GPa was achieved for thin fly ash geopolymers and fly ash/slag geopolymer, respectively in this study. Higher stiffness (0.5 GPa–31.5 GPa) was reported with thickness greater than 40 mm. With the increasing thickness, the specimen body became more rigid and was capable to withstand the load applied. This explained that high stiffness was achieved in thicker specimens. Furthermore, the incorporation of fillers and additives (such as, fibers and steel reinforcement) helped to enhance the elasticity, hardness, ultimate elongation, and energy-absorbing capacity of the specimen body which consequently contributed to higher stiffness [45]. In contrast, flexural strength was more significantly affected by other factors such as surface defects, inclusions and voids as these structural defects were the regions in which stress was concentrated [46].

3.4. *Microstructural analysis*

Fig. 6 shows the fracture surfaces of fly ash geopolymer with varying mixing parameters. With the aid of alkali activation, the spherical fly ash particles (Fig. 1a) reacted with the alkaline medium and formed geopolymer matrix which was heterogenous with presence of unreacted fly ash particles and pores. The microstructure was assessed by the homogeneity and smoothness of the matrix, pore volume, presence of cracks and crystalline phases.

Even though the formulation reached its optimal, unreacted fly ash particles and pores were still observed in the microstructure. However, the geopolymer with optimised ratio had more homogeneous, smoother and denser structure with lesser unreacted fly ash particles and pores (Fig. 6b, e and h) which led to greater flexural strength as shown in Fig. 4a–c. The presence

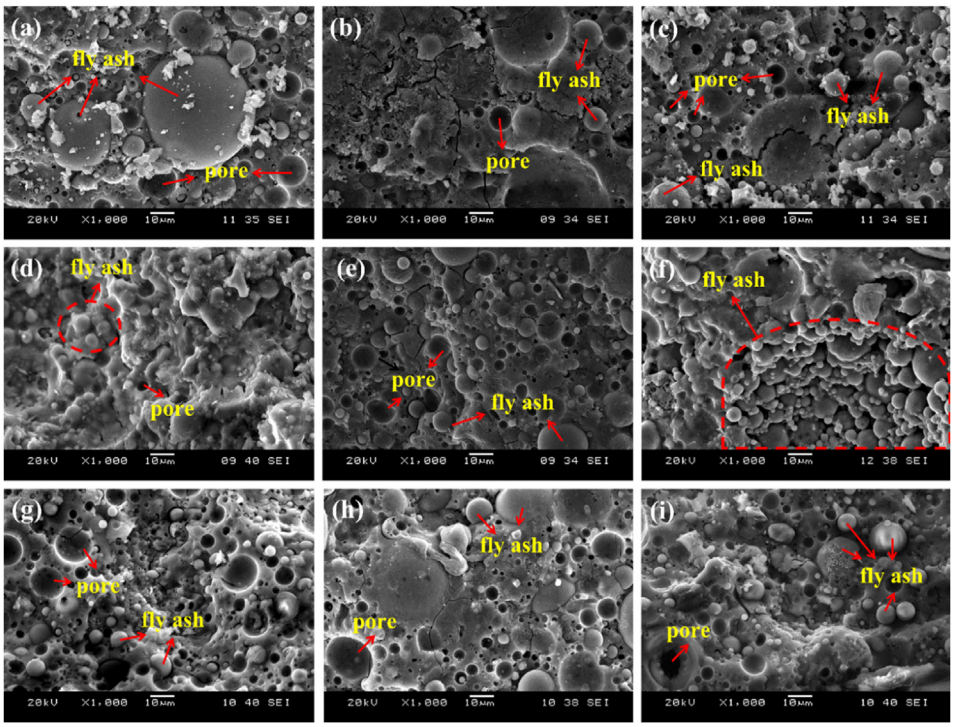

Fig. 6 – SEM micrographs of fly ash geopolymers with varying NaOH molarity (a: 8 M; b: 12 M and c: 14 M), S/L ratio (d: 1.5; e: 2.5 and f: 3.2), and Na_2SiO_3/NaOH ratio (g: 2.0; h: 4.0 and i: 4.5).

of remnant fly ash particles indicated that they did not dissolve completely in the alkali activator and further implied that geopolymerisation process was not fully complete.

Higher NaOH molarity of 12 M (Fig. 6b) produced geopolymer with smoother and more densified structure. Undissolved fly ash particles were loosely bonded to the geopolymer structure in specimen activated with lower NaOH molarity (Fig. 6a). In this context, increasing the molarity of alkali solution facilitated the formation of geopolymer matrix due to improved dissolution rate of fly ash particles. Adverse effect was observed in geopolymer activated with 14 M (Fig. 6c) as a result of disruption of geopolymerisation process due to the presence of excessive OH^- ions in geopolymer matrix, causing more pores, unreacted fly ash [30] and subsequently lower flexural strength.

Fly ash geopolymer with lower S/L ratio (Fig. 6d) possessed looser microstructure with more voids and remnant fly ash particles. Increasing S/L ratio up to 2.5 (Fig. 6e) provided sufficient amount of liquid content which increased mixture flow and contact between solid precursors with activating solution resulting in the formation of homogenous geopolymer structure [38]. However, as the S/L ratio was too high at 3.2 (Fig. 6f), huge amount of unreacted fly ash particles were present in the matrix as the liquid content was too low to initiate the geopolymerisation reaction and the excess solid content hindered the binder formation which caused a retardation in the flexural strength development (Fig. 4b).

On the other hand, increasing Na_2SiO_3/NaOH ratio increased the soluble silica content to promote the formation of geopolymer network. Hence, the microstructure became increasingly smoother and denser with less loosely-bound particles and pores (Fig. 6g and h). Raising the ratio did not improve the microstructure but became loose due to excessive sodium silicate content and highly viscous mixture.

Fig. 7 depicts the fracture surfaces of fly ash/slag geopolymers with different amounts of ladle furnace slag. The inclusion of ladle furnace slag generally increased the compactness of geopolymer structure. With the increasing amount of slag content, a densified and compact structure was observed, which complied with the bulk density and porosity measurement (Fig. 3). The increase in compactness of geopolymer structure improved the flexural strength and stiffness of fly ash/slag geopolymers (Fig. 4d) as compared to fly ash geopolymer (Fig. 4a–c). A similar observation was supported by Elyamany et al. [47] who observed a denser microstructure which consequently increased the flexural strength when 50% of GGBFS were incorporated into the fly ash geopolymer. The needle-like structure in Fig. 7c–e was corresponding to the formation of C–S–H gels which was commonly found in the geopolymer structure with high calcium precursor [55]. The coexistence of C–S–H gels with N–A–S–H gels in the geopolymer matrix helped to achieve the highest flexural strength of geopolymer as observed in Fig. 4d. This observation was supported by Pilehvar et al. [56].

3.5. *Phase analysis*

Fig. 8 illustrates the XRD pattern of raw fly ash and ladle furnace slag. Table 4 denotes the information of phases present in the samples with chemical formulation and ICDD#. A broad hump of diffraction was observed in fly ash between $2\theta = 15^\circ$ and 35°, denoting the amorphous phases of fly ash [23]. Fly ash showed an intense diffraction peak of quartz (SiO_2) with other diffraction peaks of mullite ($3Al_2O_3 \cdot 2SiO_2$)

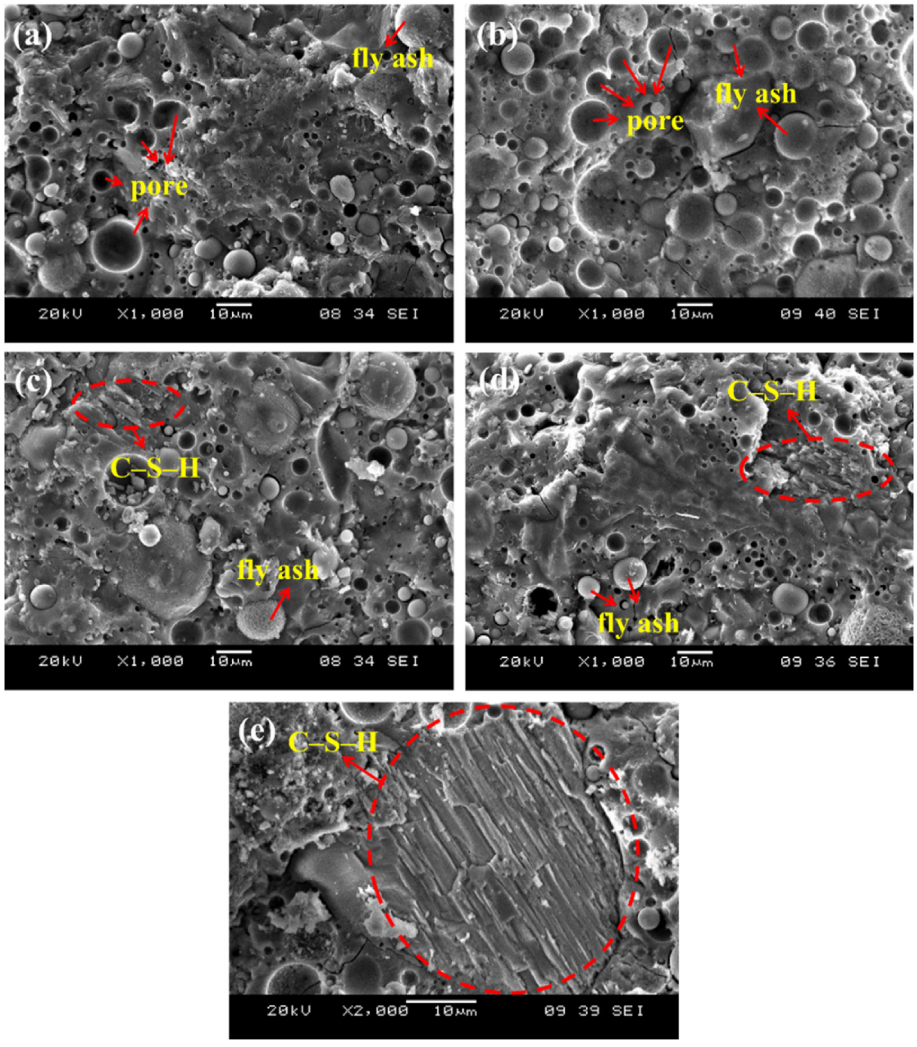

Fig. 7 – SEM micrographs of fly ash/slag geopolymers replaced with (a) 10 wt.%, (b) 20 wt.%, (c) 30 wt.%, (d) 40 wt.% of ladle furnace slag and (e) C–S–H gel in fly ash/slag geopolymer substituted with 40 wt.% of ladle furnace slag.

and hematite (Fe_2O_3). For ladle furnace slag, a predominant peak of calcio-olivine (Ca_2SiO_4) was observed with the presence of glassy phase of merwinite ($Ca_3MgSi_2O_8$), magnetite (Fe_3O_4) and calcium aluminium oxide ($CaAl_2O_4$).

Fig. 9 illustrates the XRD pattern of optimised fly ash geopolymer and fly ash/slag geopolymers with various percentages of ladle furnace slag replacement. In general, the XRD pattern of the fly ash was transformed when the fly ash was alkali-activated. The broad hump, which was attributed to the vitreous phase of the original ash, slightly shifted from 15°–30° to 20°–40° (2θ) values. This transformation indicated the formation of an alkaline aluminosilicate hydrate gel N–A–S–H which had been identified as the primary reaction product of geopolymerisation reaction in the diffraction patterns of geopolymeric materials [57]. Besides, quartz, mullite and hematite which originated from fly ash were still observed in fly ash geopolymers.

The fly ash/slag geopolymers consisted of crystalline phases from fly ash and ladle furnace slag. As the slag content increased, the intensity of the broad hump reduced because of increasing crystalline phases due to increasing slag content as well as the formation of more crystalline phases associated with the high calcium content in slag [40]. New crystalline peaks of calcite ($CaCO_3$) and calcium silicate hydrate (C–S–H) were formed with increasing slag replacement which complied with Phoo-ngernkham et al. [58] who studied fly ash/GGBFS geopolymers. The high CaO content contributed to the development of C–S–H gel and the excess CaO reacted with CO_2 and formed calcite as shown in Eqs. (5)–(7). The formation of C–S–H gel was supported by the SEM observation in Fig. 7. The increasing intensity of C–S–H and calcite was associated with the improvement of flexural strength and stiffness as shown in Fig. 4d.

$$Ca^{2+}\,(aq) + SiO_2(OH)_2^{2-}(aq) \rightarrow C-S-H\ gel\ (s) \quad (5)$$

$$Ca^{2+}\,(aq) + OH^{-}\,(aq) \rightarrow Ca(OH)_2\,(s) \quad (6)$$

$$Ca(OH)_2\,(s) + CO_2\,(g) \rightarrow CaCO_3\,(s)\ (Calcite) + H_2O \quad (7)$$

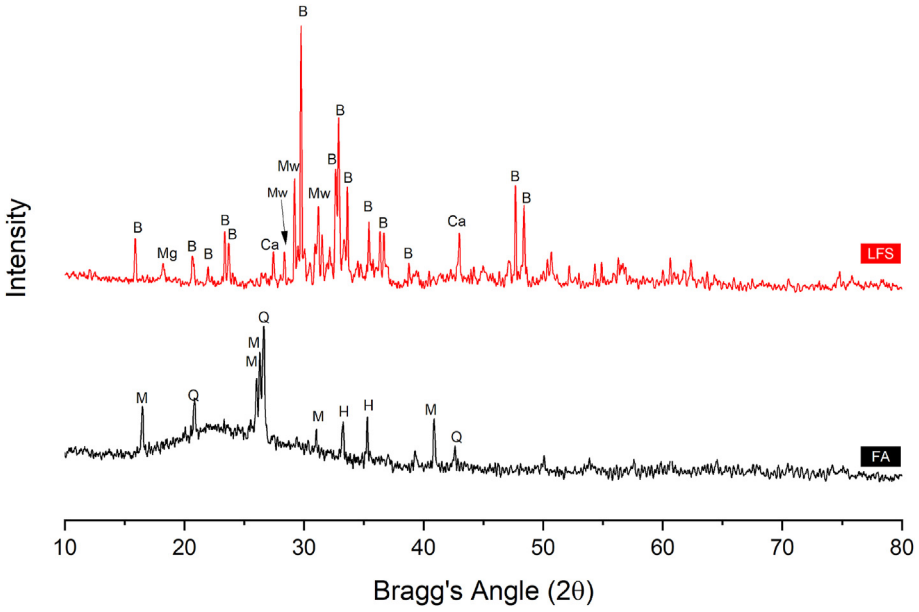

Fig. 8 – XRD diffractogram of fly ash and ladle furnace slag.

The dissolution of ladle furnace slag in alkali silicate solution is dependent on the reactivity of the ladle furnace slag and also the duration for dissolution and polycondensation before setting and hardening. It is undenied that ladle furnace slag has acceptable reactivity to act as pozzolan in geopolymer formation. The fly ash/ladle furnace slag geopolymer had a shorter setting time (1.5–3 h) compared to fly ash geopolymer without addition (5–6 h). Therefore, when the setting time was short, there was insufficient time for the dissolution of ladle furnace slag, leading to remaining slag in the geopolymer sample. This could also be proven by the XRD diffractogram which showed the presence of crystalline peaks originated from ladle furnace slag. This implied that the ladle furnace slag also acted as filler apart from acting as precursor. As mentioned above, the ladle furnace slag released Ca content for the formation of $CaCO_3$ and C–S–H. The remaining slag refined the pore structure of geopolymer by filling up voids, pores and gaps present in the geopolymer matrix [59]. On due course, the unreacted ladle furnace slag densified and reinforced the geopolymer matrix which improved the flexural strength.

3.6. *Functional group identification*

Fig. 10 represents the FTIR spectrum of fly ash, ladle furnace slag and fly ash/slag geopolymers. The main broad absorption band of fly ash was 1032 cm^{-1}, which was associated with the Si–O–T (T: Si or Al) asymmetrical stretching vibration [39]. The symmetrical vibrations of the tetrahedral linkage of Si–O or Al–O were associated with the absorption band at about 775 cm^{-1} [24]. The main peak observed for ladle furnace slag was at 858 cm^{-1}, which corresponded to the bending vibration of Ca–O and Si–O [60]. The bands at 2168 cm^{-1}, 2025 cm^{-1} and 1419 cm^{-1} corresponded to the stretching vibration of O–C–O of CO_3 group [50], which indicated the presence of carbonate minerals such as calcite in the slag.

The main band of fly ash at 1032 cm^{-1} shifted to a lower frequency (~970 cm^{-1}) in both fly ash geopolymer and fly ash/slag geopolymer, as a result of geopolymer matrix formation, whereby the Al atoms' incorporation into the tetrahedral framework [61]. The greater the shifting, the higher Al penetration degree from the glassy parts of fly ash into the $[SiO_4]^{4-}$ network and thus the geopolymeric gel was formed [6]. The

Table 4 – Denotation of phases with chemical formula and ICDD#.

Symbol	Compound	Chemical Formula	ICDD#
Q	Quartz	SiO_2	01-078-1259
M	Mullite	$3Al_2O_3 \cdot 2SiO_2$	00-006-0259
H	Hematite	Fe_2O_3	01-089-2810
B	Calcio-Olivine	Ca_2SiO_4	01-080-0941
Mw	Merwinite	$Ca_3MgSi_2O_8$	01-089-2432
Mg	Magnetite	Fe_3O_4	01-089-0950
Ca	Calcium Aluminium Oxide	$CaAl_2O_4$	01-070-0134
C	Calcite	$CaCO_3$	00-002-0623
CSH	Calcium Silicate Hydrate	$Ca_{1.5}SiO_3 \cdot 5H_2O$	00-010-0417

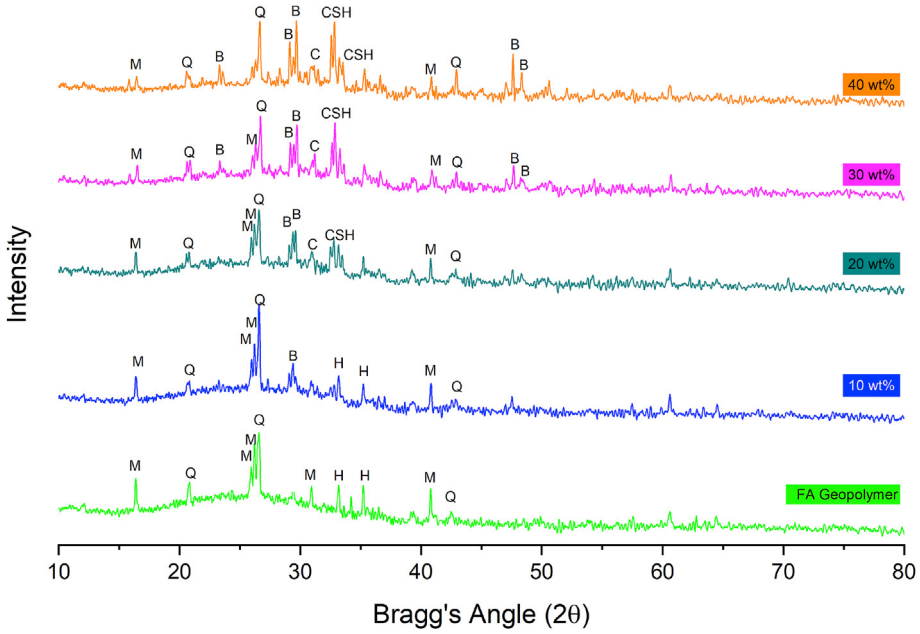

Fig. 9 – XRD diffractogram optimised fly ash geopolymer (12 M NaOH molarity, S/L ratio of 2.5 and Na_2SiO_3/NaOH ratio of 4.0) and fly ash/slag geopolymers with various percentages of ladle furnace slag replacement.

formation of this gel phase suggested the depolymerisation and structural reorganisation of amorphous phases in the fly ash geopolymer which complied with the shipment of broad hump obtained in the XRD results when fly ash was alkali-activated (Fig. 9). Furthermore, absorption bands of O–C–O stretching (~1420 cm^{-1} and ~2020 cm^{-1}) were still observed in geopolymers. The bending vibration of –OH were observed in the range of 1650 cm^{-1} [50].

The replacement of ladle furnace slag into the system further shifted the band of Si–O–Si and Si–O–Al asymmetric stretching to lower wavenumbers (973 cm^{-1} – 966 cm^{-1}). The shift to lower wavenumber indicated that the simultaneous development of cementitious gels of C–S–H and C–A–S–H gels and decreasing formation of geopolymeric gel [40]. In these systems, Ca^{2+} was supposed to be coupled with the Si–O–Al framework of geopolymeric gel, participating in the

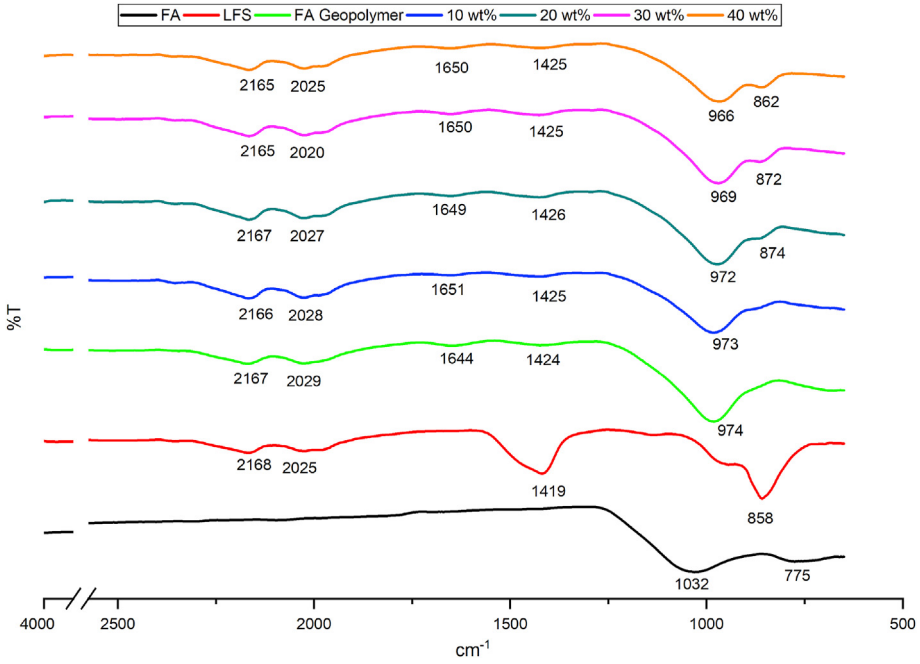

Fig. 10 – FTIR spectrum of fly ash, ladle furnace slag, fly ash geopolymer (12 M NaOH molarity, S/L ratio of 2.5 and Na_2SiO_3/NaOH ratio of 4.0) and fly ash/slag geopolymers with various percentages of ladle furnace slag replacement.

balancing of negative charge allied with tetrahedral Al (III) and replacing the alkali cations [62]. In addition, the bending vibrations of Ca–O and Si–O appeared at ~870 cm^{-1} in the fly ash/slag geopolymers replaced with 20 wt.% to 40 wt.% of ladle furnace slag. No band was detected in this region by fly ash geopolymer. This band was associated with the presence of a larger amount of CaO content from the slag [60]. As a result, the formation of C–S–H and C–A–S–H gels were favoured and thus improved the strength of geopolymers. This complied with the flexural strength obtained in Fig. 4 as the thin fly ash/geopolymers possessed a higher flexural strength than thin fly ash geopolymers.

4. Conclusion

This paper has presented the formulation and flexural properties of thin fly ash geopolymers (10 mm) and the effect of ladle furnace slag replacement on the flexural performance of thin fly ash geopolymers. The optimal formulation of thin fly ash geopolymers was 12 M NaOH molarity, S/L ratio of 2.5 and Na_2SiO_3/NaOH ratio of 4.0 led to the highest flexural strength of 6.2 MPa and stiffness of 0.14 GPa. The determining factor for flexural strength was Na_2SiO_3/NaOH ratio > S/L ratio > NaOH molarity. Geopolymer with optimised ratio exhibited more homogenous and denser structure with lesser pores results in higher flexural strength. A higher Na_2SiO_3/NaOH ratio of 4.0 was adopted for the synthesis of thin geopolymers as it could produce more viscous slurry with the desired workability which helped to retain the shape of the thin geopolymer and avoid bending. The inclusion of ladle furnace slag boosted up the flexural strength of thin fly ash geopolymer by 26% to 7.8 MPa with 40 wt.% of slag replacement as compared to pure fly ash geopolymer. The stiffness of geopolymers improved up to 0.19 GPa. The ladle furnace slag contributed as precursors and fillers simultaneously, enhancing the compactness of thin fly ash/slag geopolymer. Besides, the calcium-rich nature of ladle furnace slag facilitated the formation of C–S–H gels in the geopolymer structure which resulted in the increment of flexural strength.

A relatively similar flexural strength was obtained in this study (6.2 MPa and 7.8 MPa for fly ash geopolymers and fly ash/slag geopolymer, respectively) with the specimen thickness as thin as 10 mm, as compared to other researchers (1.4 MPa–9.9 MPa) with thickness greater than 40 mm. The Young's modulus was reduced due to the decreasing thickness. Even so, the flexural performance of thin geopolymers in this study was considerably good as the thin neat geopolymers (without the addition of fillers and aggregates) in this study exhibited high strength/thickness and higher flexural strength as compared to other researchers' geopolymer specimens without additives or fillers. The thin geopolymers have the potential to be utilised in wider range of applications such as tiles manufacturing, floor imprints, thin wall panels, roof tiles and geopolymer composite membrane. However, further work such as thermal treatment, the inclusion of fillers or additives should be carried out to improve the flexural performance of thin geopolymers to increase the versatility of thin geopolymers utilisation.

Declaration of Competing Interest

The authors declare that they have no known competing financial interests or personal relationships that could have appeared to influence the work reported in this paper.

Acknowledgement

The authors gratefully acknowledge Manjung Coal-Fired Power Plant Perak, Malaysia, and Southern Steel Berhad Penang, Malaysia for providing class F fly ash and ladle furnace slag, respectively for this research.

REFERENCES

[1] Davidovits J. Geopolymers: ceramic-like inorganic polymers. J Ceram Sci Technol 2017;8(3):335–50. https://doi.org/10.4416/jcst2017-00038.
[2] Zhang ZH, Zhu HJ, Zhou CH, Wang H. Geopolymer from kaolin in China: an overview. Appl Clay Sci 2016;119:31–41. https://doi.org/10.1016/j.clay.2015.04.023.
[3] Albidah A, Alghannam M, Abbas H, Almusallam T, Al-Salloum Y. Characteristics of metakaolin-based geopolymer concrete for different mix design parameters. J Mater Res Technol 2021;10:84–98. https://doi.org/10.1016/j.jmrt.2020.11.104.
[4] Rakhimova NR, Rakhimov RZ. Toward clean cement technologies: a review on alkali-activated fly-ash cements incorporated with supplementary materials. J Non-Cryst Solids 2019;509:31–41. https://doi.org/10.1016/j.jnoncrysol.2019.01.025.
[5] Awoyera P, Adesina A. A critical review on application of alkali activated slag as a sustainable composite binder. Case Stud Constr Mater 2019;11:e00268. https://doi.org/10.1016/j.cscm.2019.e00268.
[6] Hu Z, Wyrzykowski M, Lura P. Estimation of reaction kinetics of geopolymers at early ages. Cem Concr Res 2020;129:105971. https://doi.org/10.1016/j.cemconres.2020.105971.
[7] Davidovits J. Chemistry of geopolymeric systems, terminology. 292. In: Geopolymer, vol. 99; 1999. p. 9–39.
[8] Fan F, Liu Z, Xu G, Peng H, Cai CS. Mechanical and thermal properties of fly ash based geopolymers. Constr Build Mater 2018;160:66–81. https://doi.org/10.1016/j.conbuildmat.2017.11.023.
[9] Jamil NH, Abdullah MMAB, Che Pa F, Mohamad H, Ibrahim WMAW, Chaiprapa J. Influences of SiO_2, Al_2O_3, CaO and MgO in phase transformation of sintered kaolin-ground granulated blast furnace slag geopolymer. J Mater Res Technol 2020;9:14922–32. https://doi.org/10.1016/j.jmrt.2020.10.045.
[10] Brand AS, Fanijo EO. A review of the influence of steel furnace slag type on the properties of cementitious composites. Appl Sci-Basel 2020;10(22):8210. https://doi.org/10.3390/app10228210.
[11] Wang WC, Wang HY, Tsai HC. Study on engineering properties of alkali-activated ladle furnace slag geopolymer. Constr Build Mater 2016;123:800–5. https://doi.org/10.1016/j.conbuildmat.2016.07.068.
[12] Murri AN, Rickard WDA, Bignozzi MC, van Riessen A. High temperature behaviour of ambient cured alkali-activated

materials based on ladle slag. Cem Concr Res 2013;43:51–61. https://doi.org/10.1016/j.cemconres.2012.09.011.
[13] Nath P, Sarker PK. Flexural strength and elastic modulus of ambient-cured blended low-calcium fly ash geopolymer concrete. Constr Build Mater 2017;130:22–31. https://doi.org/10.1016/j.conbuildmat.2016.11.034.
[14] Tanyildizi H, Yonar Y. Mechanical properties of geopolymer concrete containing polyvinyl alcohol fiber exposed to high temperature. Constr Build Mater 2016;126:381–7. https://doi.org/10.1016/j.conbuildmat.2016.09.001.
[15] Raut U, Shalini A, Prabu B. Strength of geopolymer concrete reinforced with basalt fibre. Int Res J Eng Technol 2019;6(4):3811–7.
[16] Khan MI, Azizli K, Sufian S, Man Z. Sodium silicate-free geopolymers as coating materials: effects of Na/Al and water/solid ratios on adhesion strength. Ceram Int 2015;41:2794–805. https://doi.org/10.1016/j.ceramint.2014.10.099.
[17] Xu MX, He Y, Liu ZH, Tong ZF, Cui XM. Preparation of geopolymer inorganic membrane and purification of pulp-papermaking green liquor. Appl Clay Sci 2019;168:269–75. https://doi.org/10.1016/j.clay.2018.11.024.
[18] He PY, Zhang YJ, Chen H, Han ZC, Liu LC. Low-cost and facile synthesis of geopolymer-zeolite composite membrane for chromium(VI) separation from aqueous solution. J Hazard Mater 2020;392:122359. https://doi.org/10.1016/j.jhazmat.2020.122359.
[19] Kumar S, Kumar R, Kumar MB, Mehrotra SP. Process for the preparation of self-glazed geopolymer tile from fly ash and blast furnace slag. United States Patent 2007/0221100A1. 27 September 2007.
[20] Suzuk KG, Telle R, Hohmann M, Selffarth T, Kaps C, Vicent M, et al. Development of alkali-activated binder for ceramic tile production. Interceram 2012;6:350–3.
[21] Hamidi RM, Man Z, Azizli KA. Concentration of NaOH and the effect on the properties of fly ash based geopolymer. Procedia Eng 2016;148:189–93. https://doi.org/10.1016/j.proeng.2016.06.568.
[22] Kantarcı F, Türkmen İ, Ekinci E. Optimization of production parameters of geopolymer mortar and concrete: a comprehensive experimental study. Constr Build Mater 2019;228:116770. https://doi.org/10.1016/j.conbuildmat.2019.116770.
[23] Mohseni E. Assessment of Na_2SiO_3 to NaOH ratio impact on the performance of polypropylene fiber-reinforced geopolymer composites. Constr Build Mater 2018;186:904–11. https://doi.org/10.1016/j.conbuildmat.2018.08.032.
[24] Alehyen S, Achouri M, Taibi M. Characterization, microstructure and properties of fly ash-based geopolymer. J Mater Environ Sci 2017;8(5):1783–96. https://doi.org/10.1016/j.jmrt.2021.03.065.
[25] N Hui-Teng, H Cheng-Yong, L Yun-Ming, Abdullah MMAB, Ern Hun K, Razi HM, et al. Formulation, mechanical properties and phase analysis of fly ash geopolymer with ladle furnace slag replacement. J Mater Res Technol 2021;12:1212–26.
[26] Kumar EM, Ramamurthy K. Influence of production on the strength, density and water absorption of aerated geopolymer paste and mortar using Class F fly ash. Constr Build Mater 2017;156:1137–49. https://doi.org/10.1016/j.conbuildmat.2017.08.153.
[27] Görhan G, Kürklü G. The influence of the NaOH solution on the properties of the fly ash-based geopolymer mortar cured at different temperatures. Compos Part B 2014;58:371–7. https://doi.org/10.1016/j.compositesb.2013.10.082.
[28] Ghosh K, Ghosh P. Effect of $\%Na_2O$ and $\%SiO_2$ on apparent porosity and sorptivity of fly ash based geopolymer. IOSR-JEN 2012;2:96–101. https://doi.org/10.9790/3021-028196101.
[29] Leong HY, Ong DEL, Sanjayan JG, Nazari A. The effect of different Na_2O and K_2O ratios of alkali activator on compressive strength of fly ash based-geopolymer. Constr Build Mater 2016;106:500–11. https://doi.org/10.1016/j.conbuildmat.2015.12.141.
[30] Aliabdo AA, Elmoaty AEMA, Salem HA. Effect of water addition, plasticizer and alkaline solution constitution on fly ash based geopolymer concrete performance. Constr Build Mater 2016;121:694–703. https://doi.org/10.1016/j.conbuildmat.2016.06.062.
[31] Zawrah MF, Gado RA, Feltin N, Ducourtieux S, Devoille L. Recycling and utilization assessment of waste fired clay bricks (Grog) with granulated blast-furnace slag for geopolymer production. Process Saf Environ 2016;103:237–51. https://doi.org/10.1016/j.psep.2016.08.001.
[32] Ababneh FA, Alakhras AI, Heikal M, Ibrahim SM. Stabilization of lead bearing sludge by utilization in fly ash-slag based geopolymer. Constr Build Mater 2019;227:116694. https://doi.org/10.1016/j.conbuildmat.2019.116694.
[33] Song W, Zhu Z, Peng Y, Wan Y, Xu X, Pu S, et al. Effect of steel slag on fresh, hardened and microstructural properties of high-calcium fly ash based geopolymers at standard curing condition. Constr Build Mater 2019;229:116933. https://doi.org/10.1016/j.conbuildmat.2019.116933.
[34] Bignozzi MC, Manzi S, Lancellotti I, Kamseu E, Barbieri L, Leonelli C. Mix-design and characterization of alkali activated materials based on metakaolin and ladle slag. Appl Clay Sci 2013;73:78–85. https://doi.org/10.1016/j.clay.2012.09.015.
[35] De Rossi A, Simão L, Ribeiro MJ, Hotza D, Moreira RFPM. Study of cure conditions effect on the properties of wood biomass fly ash geopolymers. J Mater Res Technol 2020;9(4):7518–752. https://doi.org/10.1016/j.jmrt.2020.05.047.
[36] Zamanabadi SN, Zareei SA, Shoaei P, Ameri F. Ambient-cured alkali-activated slag paste incorporating micro-silica as repair material: effects of alkali activator solution on physical and mechanical properties. Constr Build Mater 2019;229:116911. https://doi.org/10.1016/j.conbuildmat.2019.116911.
[37] Glid M, Sobrados I, Rhaiem HB, Sanz J, Amara ABH. Alkaline activation of metakaolinite-silica mixtures: role of dissolved silica concentration on the formation of geopolymers. Ceram Int 2017;43(15):12641–50. https://doi.org/10.1016/j.ceramint.2017.06.144.
[38] Nikoloutsopoulos N, Sotiropoulou A, Kakali G, Tsivilis S. The effect of solid/liquid ratio on setting time, workability and compressive strength of fly ash based geopolymers. Mater Today: Proc 2018;5(14, Part 1):27441–5. https://doi.org/10.1016/j.matpr.2018.09.062.
[39] Samantasinghar S, Singh SP. Effect of synthesis parameters on compressive strength of fly ash-slag blended geopolymer. Constr Build Mater 2018;170:225–34. https://doi.org/10.1016/j.conbuildmat.2018.03.026.
[40] Shaikh FUA. Effects of slag content on the residual mechanical properties of ambient air-cured geopolymers exposed to elevated temperatures. J Asian Ceram Soc 2018;6(4):342–58. https://doi.org/10.1080/21870764.2018.1529013.
[41] Fang G, Ho WK, Tu W, Zhang M. Workability and mechanical properties of alkali-activated fly ash-slag concrete cured at ambient temperature. Constr Build Mater 2018;172:476–87. https://doi.org/10.1016/j.conbuildmat.2018.04.008.

[42] Gülşan ME, Alzeebaree R, Rasheed AA, Niş A, Kurtoğlu AE. Development of fly ash/slag based self-compacting geopolymer concrete using nano-silica and steel fiber. Constr Build Mater 2019;211:271–83. https://doi.org/10.1016/j.conbuildmat.2019.03.228.
[43] Cifrian E, Dacuba J, Llano T, Díaz-Fernández MDC, Andrés A. Coal fly ash–clay based geopolymer-incorporating electric arc furnace dust (EAFD): leaching behavior and geochemical modeling. Appl Sci-Basel 2021;11(2):810. https://doi.org/10.3390/app11020810.
[44] Marini P, Bellopede R, Luodes NM. Influence of thickness on flexural strength under concentrated load of natural stone in relation to EN 12372. Q J Eng Geol Hydrogeol 2017;50(4):417–21. https://doi.org/10.1144/qjegh2016-147.
[45] Yin S, Tuladhar R, Shi F, Combe M, Collister T, Sivakugan N. Use of macro plastic fibres in concrete: a review. Constr Build Mater 2015;93:180–8. https://doi.org/10.1016/j.conbuildmat.2015.05.105.
[46] Evans AG. Engineering property requirements for high performance ceramics. Mater Sci Eng 1985;71:3–21. https://doi.org/10.1016/0025-5416(85)90202-2.
[47] Elyamany HE, Elmoaty AEMA, Elshaboury AM. Setting time and 7-day strength of geopolymer mortar with various binders. Constr Build Mater 2018;187:974–83. https://doi.org/10.1016/j.conbuildmat.2018.08.025.
[48] Nazari A, Maghsoudpour A, Sanjayan JG. Flexural strength of plain and fibre-reinforced boroaluminosilicate geopolymer. Constr Build Mater 2015;76:207–13. https://doi.org/10.1016/j.conbuildmat.2014.12.002.
[49] Al-Qutaifi S, Nazari A, Bagheri A. Mechanical properties of layered geopolymer structures applicable in concrete 3D-printing. Constr Build Mater 2018;176:690–9. https://doi.org/10.1016/j.conbuildmat.2018.04.195.
[50] Mucsi G, Szenczi Á, Nagy S. Fiber reinforced geopolymer from synergetic utilization of fly ash and waste tire. J Clean Prod 2018;178:429–40. https://doi.org/10.1016/j.jclepro.2018.01.018.
[51] Saafi M, Tang L, Fung J, Rahman M, Liggat J. Enhanced properties of graphene/fly ash geopolymeric composite cement. Cement Concr Res 2015;67:292–9. https://doi.org/10.1016/j.cemconres.2014.08.011.
[52] Adak D, Sarkar M, Mandal S. Effect of nano-silica on strength and durability of fly ash based geopolymer mortar. Constr Build Mater 2014;70:453–9. https://doi.org/10.1016/j.conbuildmat.2014.07.093.
[53] Bhutta A, Borges PHR, Zanotti C, Farooq M, Banthia N. Flexural behavior of geopolymer composites reinforced with steel and polypropylene macro fibers. Cem Concr Compos 2017;80:31–40. https://doi.org/10.1016/j.cemconcomp.2016.11.014.
[54] Luhar S, Chaudhary S, Luhar I. Development of rubberized geopolymer concrete: strength and durability studies. Constr Build Mater 2019;204:740–53. https://doi.org/10.1016/j.conbuildmat.2019.01.185.
[55] Kurtoğlu AE, Alzeebaree R, Aljumaili O, Niş A, Gülşan ME, Humur G, et al. Mechanical and durability properties of fly ash and slag based geopolymer concrete. Adv Concr Constr 2018;6(4):345–62. https://doi.org/10.12989/acc.2018.6.4.345.
[56] Pilehvar S, Cao VD, Szczotok AM, Carmona M, Valentini L, Lanzón M, et al. Physical and mechanical properties of fly ash and slag geopolymer concrete containing different types of micro-encapsulated phase change materials. Constr Build Mater 2018;173:28–39. https://doi.org/10.1016/j.conbuildmat.2018.04.016.
[57] Li X, Ma X, Zhang S, Zheng E. Mechanical properties and microstructure of class C fly ash-based geopolymer paste and mortar. Mater-Basel 2013;6(4):1485–95. https://doi.org/10.3390/ma6041485.
[58] Phoo-ngernkham T, Maegawa A, Mishima N, Hatanaka S, Chindaprasirt P. Effects of sodium hydroxide and sodium silicate solutions on compressive and shear bond strengths of FA–GBFS geopolymer. Constr Build Mater 2015;91:1–8. https://doi.org/10.1016/j.conbuildmat.2015.05.001.
[59] Kürklü G. The effect of high temperature on the design of blast furnace slag and coarse fly ash-based geopolymer mortar. Compos Part B 2016;92:9–18. https://doi.org/10.1016/j.compositesb.2016.02.043.
[60] Guetteche MN, Zergua A, Hannachi S. Investigating the local granulated blast furnace slag. Open J Civil Eng 2012;2(1):10–5. https://doi.org/10.4236/ojce.2012.21002.
[61] Nikolov A, Nugteren H, Rostovsky I. Optimization of geopolymers based on natural zeolite clinoptilolite by calcination and use of aluminate activators. Constr Build Mater 2020;243:118257. https://doi.org/10.1016/j.conbuildmat.2020.118257.
[62] Lodeiro IG, Fernández-Jimenez A, Palomo A, Macphee DE. Effect on fresh C-S-H gels of the simultaneous addition of alkali and aluminium. Cem Concr Res 2010;40(1):27–32. https://doi.org/10.1016/j.cemconres.2009.08.004.